AIP | Applied Physics Letters

Molecular dynamics simulation of Lorentz force microscopy in magnetic nano-disks

R. A. Dias, E. P. Mello, P. Z. Coura, S. A. Leonel, I. O. Maciel, D. Toscano, J. C. S. Rocha, and B. V. Costa

Citation: Applied Physics Letters **102**, 172405 (2013); doi: 10.1063/1.4803474
View online: http://dx.doi.org/10.1063/1.4803474
View Table of Contents: http://scitation.aip.org/content/aip/journal/apl/102/17?ver=pdfcov
Published by the AIP Publishing

Articles you may be interested in

Nano-crystallization and magnetic mechanisms of Fe85Si2B8P4Cu1 amorphous alloy by ab initio molecular dynamics simulation
J. Appl. Phys. **115**, 173910 (2014); 10.1063/1.4875483

Material dependence of magnetic force microscopy performance using carbon nanotube probes: Experiments and simulation
J. Appl. Phys. **115**, 093907 (2014); 10.1063/1.4867738

Thermal behavior of superparamagnetic cobalt nanodots explored by anisotropic magnetic molecular dynamics simulations
J. Appl. Phys. **111**, 07D126 (2012); 10.1063/1.3677932

High field-gradient dysprosium tips for magnetic resonance force microscopy
Appl. Phys. Lett. **100**, 013102 (2012); 10.1063/1.3673910

Magnetic vortex formation and gyrotropic mode in nanodisks
J. Appl. Phys. **109**, 014301 (2011); 10.1063/1.3526970

Confidently measure down to 0.01 fA and up to 10 PΩ
Keysight B2980A Series Picoammeters/Electrometers
View video demo›
KEYSIGHT TECHNOLOGIES

This article is copyrighted as indicated in the article. Reuse of AIP content is subject to the terms at: http://scitation.aip.org/termsconditions. Downloaded to IP: 150.164.14.44 On: Wed, 04 Feb 2015 21:44:10

Molecular dynamics simulation of Lorentz force microscopy in magnetic nano-disks

R. A. Dias,[1,a)] E. P. Mello,[1] P. Z. Coura,[1] S. A. Leonel,[1] I. O. Maciel,[1] D. Toscano,[1] J. C. S. Rocha,[2] and B. V. Costa[2]
[1]*Departamento de Física, ICE, UFJF, 36036-330, Juiz de Fora, MG, Brazil*
[2]*Departamento de Física, Laboratório de Simulação, ICEX, UFMG, 30123-970, Belo Horizonte, MG, Brazil*

(Received 11 March 2013; accepted 15 April 2013; published online 2 May 2013)

In this paper, we present a molecular dynamics simulation to model the Lorentz force microscopy experiment. Experimentally, this technique consists in the scattering of electrons by magnetic structures in surfaces and gases. Here, we will explore the behavior of electrons colliding with nano-magnetic disks. The computational molecular dynamics experiment allows us to follow the trajectory of individual electrons all along the experiment. In order to compare our results with the experimental one reported in literature, we model the experimental electron detectors in a simplified way: a photo-sensitive screen is simulated in such way that it counts the number of electrons that collide at a certain position. The information is organized to give in grey scale the image information about the magnetic properties of the structure in the target. Computationally, the sensor is modeled as a square matrix in which we count how many electrons collide at each specific point after being scattered by the magnetic structure. We have used several configurations of the magnetic nano-disks to understand the behavior of the scattered electrons, changing the orientation direction of the magnetic moments in the nano-disk in several ways. Our results match very well with the experiments, showing that this simulation can become a powerful technique to help to interpret experimental results. © *2013 AIP Publishing LLC* [http://dx.doi.org/10.1063/1.4803474]

Parallel with the increasing use of magneto-electronic based devices, such as MRAMs (Magneto-resistive Random access Memory), there was a consequent increase in the need for understanding of magnetization processes in micrometric and nanometric scale. Due to the complexity of the phenomena involved, much of the work done so far is mainly based in numerical simulations such as the micro-magnetic modeling (MMC).[1,2] This technique became an important tool for understanding the dynamic of magnetization in thin films, finite nano-structures, and many others,[3] and it has helped to guide the engineering of materials in developing and improving applications, such as mechanisms for storing information in magnetic electronic devices.

One of the most promising applications in MRAMs technology is the vortex like structure that appears in nano-disk systems under certain conditions.[4] The magnetic vortex structure can be understood as the stream lines of a fluid in a sink hole with the magnetic moments being tangent to the stream lines. In the vortex core, the magnetic moments minimize the energy of the system by turning out of the plane. The out-of-plane structure is twofold degenerated presenting two configurations: "up" or "down" with polarization, $p = +1, -1$, respectively. To flip the system from $p = +1$ to $p = -1$ configuration, a huge energy barrier has to be overcome,[5] which makes the system very stable. It is believed that the "up" or "down" configurations can be used to store a bit of information. Some authors have carried out theoretical as well as experimental[6–8] studies suggesting that a creation-annihilation vortex/anti-vortex process mediates the switching. Today, there is a large amount of techniques such as Magnetic Force Microscopy (MFM),[9] Transmission Lorentz Force Microscopy (TLFM),[10–12] Spin Polarized Electron Microscopy,[13] X-ray magnetic circular dichroism,[14] and many others[15,16] that are being used to build and characterize of such devices.

In this work, we present a theoretical and computational model to reproduce the results experimentally obtained from the TLFM.[10] Although all of our effort is dedicated to describe the TLFM experiment, the main aspects of our simulation are quite general. In fact, our work is driven by the following question: "Can we reproduce the experimental electron scattering results for nano-magnetic structures, in the context of TLFM, using classical molecular dynamics simulations?" In particular, we are interested in the study of the vortex core structure in nano-scale disks. In spite of our approach, it has been shown by Mansuripur[17] that the physical mechanism that governs all known modes of Lorentz force microscopy is an interaction, commonly known as Aharonov-Bohm effect,[18] resulting in a phase shift directly proportional to the path integral of the vector potential that can be written as a 2*D* Fourier series. This kind of approach has been used successfully by many authors[19–21] to model the TLFM results of magnetic thin films and nano-structures.

The TLFM, in a simplified way, is a experimental technique where electrons are scattered by a magnetic thin film due to the Lorentz force.[22] There are several experimental modes to observe the phase shift acquired by the scattered electrons. These modes are typically: Fresnel, Foucault, Differential Phase Contrast, Small Angle Diffraction, Electron Interference, and Holography. In other words, these modes are simply different designs for capturing the information contained in the phase of the beam after it is scattered by the magnetic sample.[17,23]

In this work, we will focus on the Fresnel mode of the Lorentz force microscopy that can be used to probe the

a)radias@fisica.ufjf.br

 © 2013 AIP Publishing LLC

This article is copyrighted as indicated in the article. Reuse of AIP content is subject to the terms at: http://scitation.aip.org/termsconditions. Downloaded to IP: 150.164.14.44 On: Wed, 04 Feb 2015 21:44:10

in-plane magnetization pattern of the nano-structures. In this technique, an incoming electron beam is deflected by the in-plane components of the magnetization of the sample. Domain walls, for example, become visible as black or white lines, depending on the defocus (over or under-focus) and the succession of the local magnetization. The goal here is to show that Molecular Dynamics can help us to interpret the results of the experiment without any ambiguity.

We start writing the Hamiltonian, $\mathcal{H}$, for N non-interacting charged particles q_i, with mass m_i, in an electromagnetic field, given by:

$$\mathcal{H} = \sum_{i=1}^{N} \frac{1}{m_i}\left(\vec{p}_i - q_i\vec{A}(r_i,t)\right)^2 + q_i\phi(r_i), \tag{1}$$

where $\vec{A}(r_i,t)$ is the magnetic potential vector, $\phi(r_i)$ is the scalar potential, $m_i = m_e$ is the electron mass, $q_i = -e$ is the fundamental charge, and $\vec{p}_i$ is the momentum of the ith electron. As a matter of simplification, we do not consider the electronic spin.

From the non-relativistic Hamilton equation of motion, we obtain

$$m_e\frac{d^2\vec{r}_i}{dt^2} = -e[\vec{E}(r_i,t) + \vec{v}_i \times \vec{B}(r_i,t)] = \vec{F}_i^{Lorentz}, \tag{2}$$

where

$$\vec{B}(r_i,t) = \nabla_i \times \vec{A}(r_i,t) \tag{3}$$

and

$$\vec{E}(r_i,t) = -\nabla\phi(r_i) - \frac{\partial\vec{A}(r_i,t)}{\partial t} \tag{4}$$

are the magnetic and electric fields, respectively. To evolve in time the equations of motion, we have set an appropriate initial condition and integrated forward in time, a discretized version of the equations of motion, using the Adams-Molton predictor corrector method.[24] In the target, we consider that the magnetic domains are electrically neutral, localized at fixed positions $\vec{r}_i$ with magnetic moment $\vec{m}_j$. The potential magnetic vector $\vec{A}(r_i)$ and the electrostatic potential $\phi(r_i)$ are defined by,

$$\vec{A}(r_i,t) = \frac{\mu_0}{4\pi}\sum_{j=1}^{M}\frac{\vec{m}_j \times \vec{r}_{ij}}{r_{ij}^3}, \tag{5}$$

and

$$\phi(r_i) = \frac{e}{4\pi\epsilon_0}\left[\phi_0 z_i + \sum_{j=1}^{M}\frac{e^{-\frac{r_{ij}}{\lambda}}}{r_{ij}}\right]. \tag{6}$$

The first term of the electrostatic potential in Eq. (6) represents a constant potential in the $\hat{z}$ direction, where ϕ_0 control the potential intensity, and ϵ_0 is the permittivity of free space. The second term is the Yukawa potential,[25] where λ controls the range of the potential.

Using Eqs. (3) and (4), we obtain the magnetic and electric field in a given position as

$$\vec{B}(r_i,t) = -\frac{\mu_0}{4\pi}\sum_j\left[\frac{\vec{m}_j}{r_{ij}^3} - \frac{3\vec{r}_{ij}(\vec{m}_j\cdot\vec{r}_{ij})}{r_{ij}^5}\right] \tag{7}$$

and

$$\vec{E}(r_i,t) = \frac{e}{4\pi\epsilon_0}\left[\sum_{j=1}^{M}\frac{e^{-\frac{r_{ij}}{\lambda}}}{r_{ij}^2}\left(\frac{\vec{r}_{ij}}{\lambda} + \frac{\vec{r}_{ij}}{r_{ij}}\right) - \phi_0\hat{z}\right], \tag{8}$$

respectively.

Let us consider an arrangement of magnetic moments, $\vec{m}(\vec{r}_j) = \vec{m}_j$, distributed in the sites of a square lattice forming a disk of radius R_d and thickness L_z, as shown in Figure 1. Each site has a volume $V_{cell} = a_0^3$, a_0 being the space discretization. The magnetic moment of each site represents a coarse graining of the system such that $\vec{m}_j = \sum_{cell}\vec{\mu} = m_{cell}\vec{S}(\vec{r}_j)$, where $\vec{\mu}$ is the microscopic magnetic moment. The module $|\vec{m}_j| = m_{cell} = M_s V_{cell}$ and M_s is the saturation magnetization of the material. We use a spherical parametrization for the direction of the magnetic moments,

$$\vec{S}_j = \cos(\Theta_j)\cos(\Phi_j)\hat{x} + \cos(\Theta_j)\sin(\Phi_j)\hat{y} + \sin(\Theta_j)\hat{z}.$$

As initial condition, we distribute the electrons with zero velocities in random positions inside a circle of radius $R_f = 2R_d$ in the plane $z_d = 20a_0$ above the nano-disk. The units of length, time, and energy are a_0, $\gamma = \sqrt{4\pi\varepsilon_0 a_0^3 m_e}/e$ and $E_0 = e/4\pi\varepsilon_0 a_0$, respectively. Considering that the disk is made of Permalloy-79 with the saturation magnetization given by $M_s = 8.6\times10^5 A/m$ and exchange stiffness constant $A = 13pJm^{-1}$, we obtain an exchange length $\lambda_{ex} = \sqrt{2A/\mu_0 M_s^2} = 5.3\,\text{nm}$. Using the λ_{ex} as a maximum scale length, we set $a_0 = 5.0\,\text{nm} < \lambda_{ex}$ to ensure that all microscopic magnetic moment $\vec{\mu}$ in each site are aligned because the exchange interaction. Using this parameters, we obtain the time unit as $\gamma = 0.022217\,\text{ps}$ and energy $E_0 = 0.28796\,\text{eV}$. The disk thickness is set to $L_z = a_0$, the Yukawa potential parameter is $\lambda = 0.5a_0$, and the external potential strength is $\phi_0 = 11.0\,\text{nm}^{-2}$.

The electron sensor is modeled as a discrete matrix of dimension $(N_x \times N_y)$, with cell size $(\Delta x, \Delta y)$ and we use

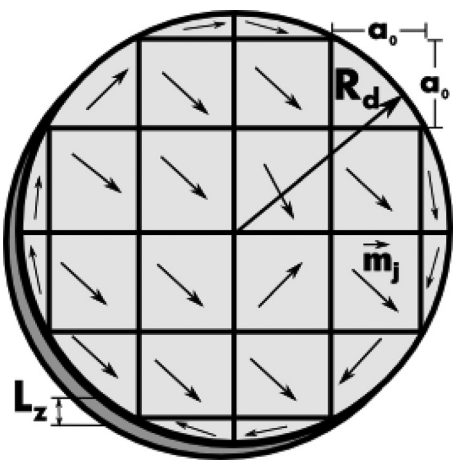

FIG. 1. Schematic picture showing the regular arrangement of magnetic moments distributed in a disk of radius R_d and thickness L_z.

This article is copyrighted as indicated in the article. Reuse of AIP content is subject to the terms at: http://scitation.aip.org/termsconditions. Downloaded to IP: 150.164.14.44 On: Wed, 04 Feb 2015 21:44:10

$\Delta x = \Delta y = 0.5a_0$. Every time that an electron reaches the interval $[(x_i, y_j), (x_i + \Delta x, y_j + \Delta y)]$, we add one count to the matrix counter, building an intensity map.

Initially, we studied a nano-disk of radius $R_d = 75\,\text{nm}$ with uniform magnetization in the positive x direction, defined by $\Theta_j = 0$ and $\Phi_j = 0$, as shown in Figure 2(a). A schematic view of the velocity, magnetic force, and magnetic field that a electron feels in that position is also showed. In Figure 2(b), we show the simulation result where we used $N = 4 \times 10^5$ particles to build the map, where brighter regions indicate larger number of electrons. As should be expected, the upper region is brighter than the lower one, indicating that electrons preferentially scatter to the upper regions due to the magnetic force. Figure 2(c) shows the transverse profile at the position $x = 0$. We note that for values of $y > 0$, the intensity is higher and quite constant, compared with values of $y < 0$.

As a second example, we use a disk of radius $R_d = 75\,\text{nm}$ with a planar clockwise vortex state defined by $\Theta_j = 0$ and $\Phi_j = -\frac{\pi}{2} + \arctan(\frac{y_j - y_0}{x_j - x_0})$, where $(x_0, y_0) = (0, 0)$ is the position of the vortex core. A schematic view of the simulation arrangement is shown in Figure 3(a). Figure 3(b) shows the simulation results for $N = 1.2 \times 10^6$ electrons. The central region is darker, indicating that the majority of the electrons scattered far way from the vortex center. The figure is radially symmetric due the vortex geometry. Figure 3(c) shown the transverse profile at position $x = 0$ showing a dip of intensity around the position $y = 0$. This simulation agrees quite well with experimental results as well as with theoretical results[19,21,26] in the literature. This magnetic state works for electrons as a divergent lens.

If we use a counterclockwise vortex, the dark-bright regions exchange place as shown in Figures 3(d)–3(f). In opposite way as in the clockwise vortex, this magnetic state works for electrons as a convergent lens.

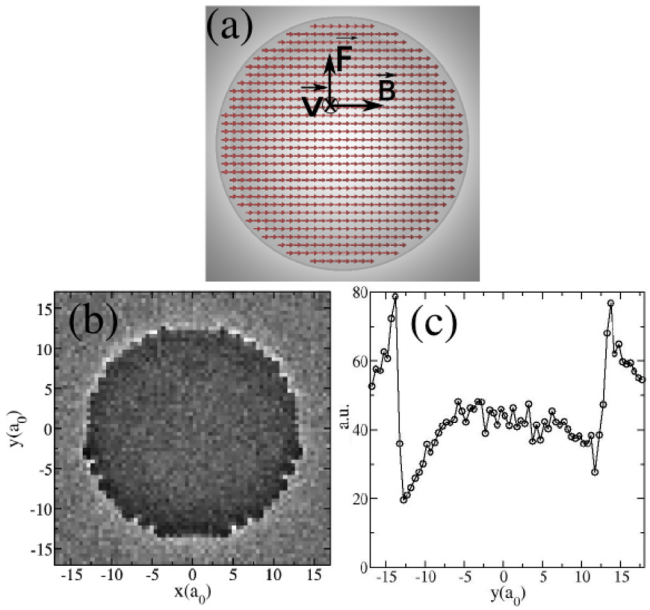

FIG. 2. (a) Magnetic simulated configuration of the disk of radius $R_d = 75\,\text{nm}$ and with uniform magnetization. (b) Simulation result presenting an upper region brighter than the lower one as expected, if one considers the direction of the magnetic force. (c) Transverse line profile at the position $x = 0$.

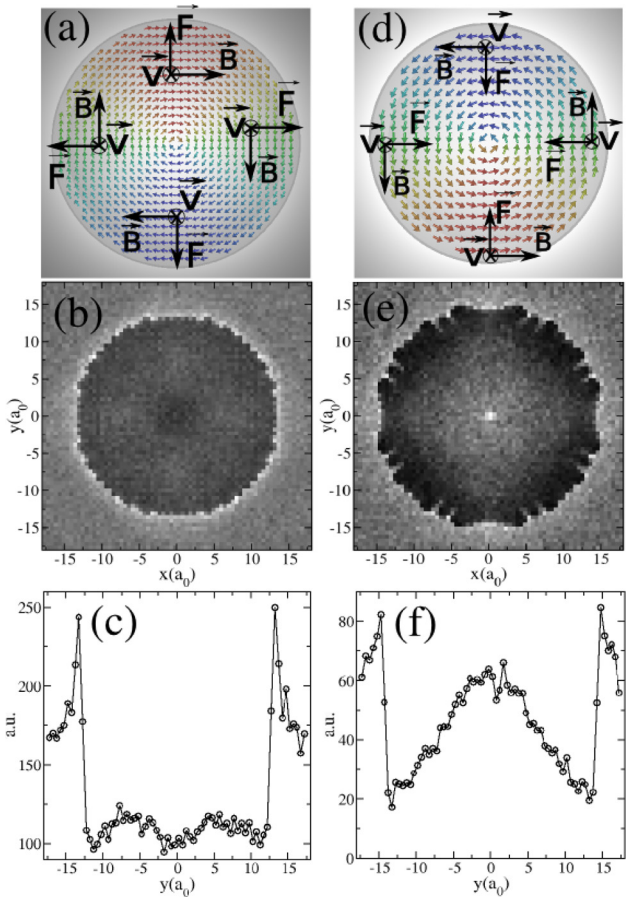

FIG. 3. (a) Magnetic simulated configuration of a disk of radius $R_d = 75\,\text{nm}$ and with a clockwise vortex. (b) Simulation result presenting a central darker region indicating that most of the electrons scatter far way from the vortex center. (c) Transverse profile at position $x = 0$ showing a dip of intensity around center of the vortex. (d) Magnetic simulated configuration of a disk of radius $R_d = 50\,\text{nm}$ and with a counterclockwise vortex (e) Simulation result presenting a central brighter region indicating that the most number of electrons scatter to the center of the disk and vortex center. (f) Transverse profile at position $x = 0$ showing a higher intensity around center of the vortex.

Figures 4(a) and 4(b) shows a similar result for the vortex fixed out of the center, $(x_0, y_0) = (-6, 6)a_0$. In this case, most of the electrons scatter to the center of the vortex. The fact the darker/brighter center of the image is in the same position of the center of the vortex was used by experimentalists[26] to track the vortex position in a disk under a external applied magnetic field.

In the next two studied cases, we set a nano-disk of radius $R_d = 50\,\text{nm}$ with two planar anti-vortex states. This magnetic states are defined by $\Phi_j = \pm\pi/2 - \arctan(\frac{y_j - y_0}{x_j - x_0})$, $\Theta_j = 0$, with $(x_0, y_0) = (0, 0)$, where $\pm\pi/2$ are, respectively, the states showed in Figures 5(a) and 5(d). Figures 5(b) and 5(e) show the results for the simulations of the Figures 5(a) and 5(d), respectively. In both cases, we use $N = 4 \times 10^5$ electrons to build the image maps. We observe in those figures a bright central region located in the position of the anti-vortex core, indicating that an appreciable number of electrons were scattered in the direction of the anti-vortex center. However, we note that the images present an anisotropy characterized by a spread, or enlargement, in the horizontal $(-\pi/2)$ or vertical $(+\pi/2)$ directions depending on the sense of rotation. Figures 5(c) and 5(f) shows the

This article is copyrighted as indicated in the article. Reuse of AIP content is subject to the terms at: http://scitation.aip.org/termsconditions. Downloaded to IP: 150.164.14.44 On: Wed, 04 Feb 2015 21:44:10

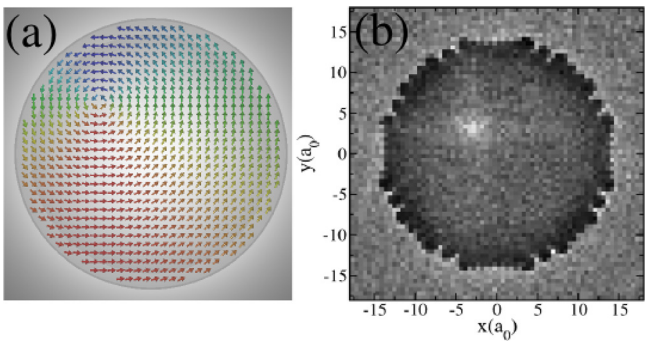

FIG. 4. (a) Magnetic simulated configuration of a disk of radius $R_d = 75$ nm and with a counterclockwise vortex out of the disk center. (b) Simulation result presenting a brighter region indicating that most of the electrons scatter to the vortex center.

transverse profile at the position $x = 0$. The electrons from the top and bottom part of the disk spread to the center of the anti-vortex while electrons from the left and right sides spread out of the anti-vortex center. A similar behavior is seen in Figure 5(d) with an inversion of the forces. As a counterclockwise vortex or $(\pm\pi/2)$ anti-vortex give the same bright spot, they cannot be distinguished if the anisotropy is not detected. In this sense, these magnetic states are indistinguishable with TLFM.

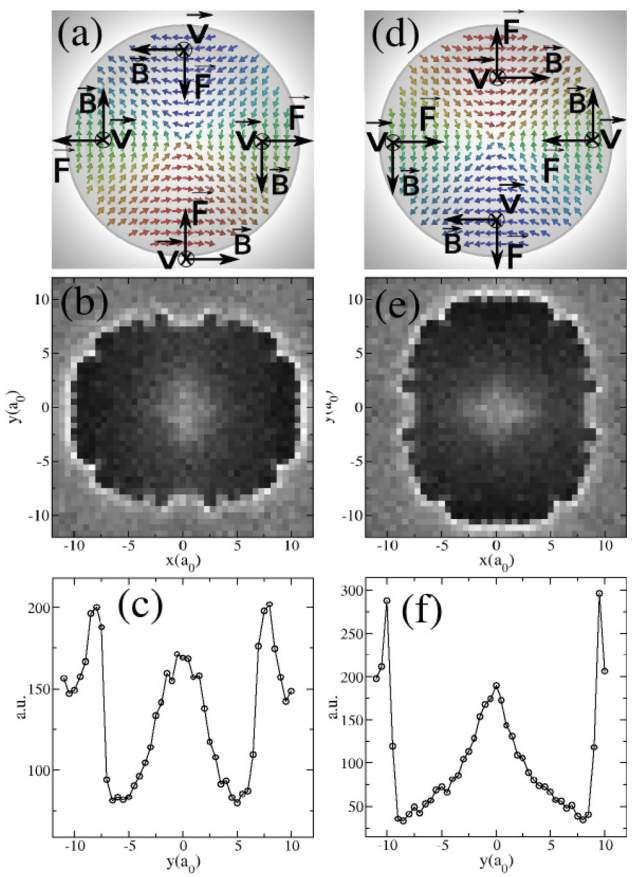

FIG. 5. (a) Magnetic simulated configuration of a disk of radius $R_d = 50$ nm and with a $\Phi_j = +\pi/2 - \arctan(\frac{y_j - y_0}{x_j - x_0})$ anti-vortex. (b) Simulation result and (c) transverse profile at position $x = 0$ indicating that the most number of electrons scatter to the anti-vortex center. (d) Magnetic simulated configuration of a disk of radius $R_d = 50$ nm and with a $\Phi_j = -\pi/2 - \arctan(\frac{y_j - y_0}{x_j - x_0})$ anti-vortex. (e) Simulation result and (f) transverse profile at position $x = 0$ also indicating that the most number of electrons scatter to the anti-vortex center.

In this work, we simulate the Transmission Lorentz force microscopy using the technique of classical molecular dynamics. Our simulation predicts quite well the behavior described in the literature. We observed that the magnetic nano-disks which have states of vortex or anti-vortex act as a convergent or divergent lens for electrons, depending on the direction of rotation. We observe a bright spot in the center of the anti-vortex state for both $(\pm\pi/2)$ state. An anisotropy in the images for anti-vortex states with $(\pm\pi/2)$ state are also observed. Based in this conclusion, if one uses a TLFM experiment to study a flip from $p = +1$ to $p = -1$ polarizations mediated by a creation-annihilation vortex anti-vortex process, one cannot distinguish the presence of this magnetic structures. Finally, this simulation program can be useful to analyze TLFM results and it is a freely open code available with the authors.

This work was partially supported by the Brazilian agencies CNPq and FAPEMIG. Numerical works were done at the Laboratório de Simulação Computacional do Departamento de Física da UFJF.

[1]J. Fidlera, D. Suessa, and T. Schrefl, *Handbook of Magnetic Materials* (Elsevier, 2006), Vol. 16.
[2]D. Toscano, S. A. Leonel, R. A. Dias, P. Z. Coura, J. C. S. Rocha, and B. V. Costa, J. Appl. Phys. **109**, 014301 (2011).
[3]A. P. Guimaraes, "Principles of Nanomagnetism," in *NanoScience and Technology* (Springer, Berlin, 2009).
[4]W. Zhang, R. Singh, N. Bray-Ali, and S. Haas, Phys. Rev. B **77**, 144428 (2008).
[5]J. Caputo, Y. Gaididei, F. G. Mertens, and D. D. Sheka, Phys. Rev. Lett. **98**, 056604 (2007).
[6]J.-S. Yang, C.-M. Lee, and C.-R. Chang, IEEE Trans. Magn. **47**, 641–644 (2011).
[7]B. Van Waeyenberge, A. Puzic, H. Stoll, K. W. Chou, T. Tyliszczak, R. Hertel, M. Faehnle, H. Brueckl, K. Rott, G. Reiss, I. Neudecker, D. Weiss, C. H. Back, and G. Schuetz, Nature **444**, 461–464 (2006).
[8]Q. F. Xiao, J. Rudge, B. C. Choi, Y. K. Hong, and G. Donohoe, Appl. Phys. Lett. **89**, 262507 (2006).
[9]T. Shinjo, T. Okuno, R. Hassdorf, K. Shigeto, and T. Ono, Science **289**, 930–932 (2000).
[10]J. Raabe, R. Pulwey, R. Sattler, T. Schweinböck, J. Zweck, and D. Weiss, J. Appl. Phys. **88**, 4437–4439 (2000).
[11]M. Schneider, H. Hoffmann, and J. Zweck, Appl. Phys. Lett. **79**, 3113–3115 (2001).
[12]M. Schneider, H. Hoffmann, S. Otto, Th. Haug, and J. Zweck, J. Appl. Phys. **92**, 1466–1472 (2002).
[13]A. Wachowiak, J. Wiebe, M. Bode, O. Pietzsch, M. Morgenstern, and R. Wiesendanger, Science **298**, 577–580 (2002).
[14]P. Fischer, G. Denbeaux, T. Eimuller, D. Goll, and G. Schutz, IEEE Trans. Magn. **38**, 2427–2431 (2002).
[15]S.-H. Chung, R. D. McMichael, D. T. Pierce, and J. Unguris, Phys. Rev. B **81**, 024410 (2010).
[16]R. P. Cowburn, D. K. Koltsov, A. O. Adeyeye, M. E. Welland, and D. M. Tricker, Phys. Rev. Lett. **83**, 1042–1045 (1999).
[17]M. Mansuripur, J. Appl. Phys. **69**, 2455–2464 (1991).
[18]Y. Aharonov and D. Bohm, Phys. Rev. **115**, 485–491 (1959).
[19]D.-T. Ngo and S. McVitie, Ultramicroscopy **111**, 1276–1285 (2011).
[20]T. Haug, S. Otto, M. Schneider, and J. Zweck, Ultramicroscopy **96**, 201–206 (2003).
[21]C. Phatak, M. Tanase, A. K. Petford-Long, and M. De Graef, Ultramicroscopy **109**, 264–267 (2009).
[22]J. D. Jackson, *Classical Electrodynamics*, 3rd ed. (Wiley, 1998).
[23]M. De Graef and Y. Zhu. "Magnetic imaging and its applications to materials," in *Experimental Methods in the Physical Sciences* (Academic Press, 2001).
[24]S. E. Koonin and D. C. Meredith, *Computational Physics: Fortran Version* (Westview Press, 1998).
[25]G. E. Brown and A. D. Jackson, *The Nucleon-Nucleon Interaction* (North-Holland Publishing, Amsterdam, 1976).
[26]M. Schneider, H. Hoffmann, and J. Zweck, Appl. Phys. Lett. **77**, 2909–2911 (2000).

This article is copyrighted as indicated in the article. Reuse of AIP content is subject to the terms at: http://scitation.aip.org/termsconditions. Downloaded to IP: 150.164.14.44 On: Wed, 04 Feb 2015 21:44:10